Journal of Engineering Physics and Thermophysics, Vol. 83, No. 4, 2010

HEAT TRANSFER AND HYDRODYNAMICS IN THE FIELDS OF MASS FORCES

A. A. Khalatov

UDC 536.27

A brief review of the investigations in the field of heat transfer and hydrodynamics in the fields of mass forces carried out at the Institute of Applied Thermal Physics of the National Academy of Sciences of Ukraine is presented. The review is devoted to swirling flows, near convex and concave surfaces, in surface-vortex systems of various configurations.

Keywords: *heat transfer, hydrodynamics, swirling flow, convex and concave surfaces, surface-vortex systems.*

Introduction. Flows in the fields of mass forces — swirling and curved flows, flows near surface-vortex systems, in nozzle blocks, curvilinear channels, and in rotating systems — form the thermal basis of many working processes in thermal power engineering, power plant engineering, mechanical engineering, and chemical technology. Such flows have a complex structure, are three-dimensional and transient, and in them secondary and vortex flows are initiated. The technological development, the growth of the operating parameters of devices, and the complication of the structure of the flows in them call for more detailed fundamental research, studies of the specific features of the heat transfer and hydrodynamics in the fields of mass forces, and the development on this basis of more exact models and computing methods.

In 1983, such investigations were commenced at the Institute of Applied Thermal Physics of the National Academy of Sciences of Ukraine (IATP, National Academy of Sciences of Ukraine) in cooperation with leading Ukrainean and Russion institutions in the field of aircraft engine engineering, power plant engineering, mechanical engineering, and chemical technology. Part of the research program was carried out in laboratories of the University of Cardiff (Great Britain), State Universities of Minnesota and Utah (USA), and of the US Air Force Academy. The research program includes detailed studies of five groups of flows in the fields of mass forces: 1) swirling flows in channels, 2) flows on convex and concave surfaces, 3) flows in nozzle blocks of gas turbines with vortex structures, 4) flows in surface-vortex systems, and 5) flows in rotating systems. Below we present the most important results obtained at the IATP, National Academy of Sciences of Ukraine for the first three groups of flows [1–7]. The results of investigations of the heat transfer and hydrodynamics in nozzle blocks of gas turbines with vortex structures and in rotating systems are presented in monographs [8, 9].

1. Swirling Flows [1–4]. The program of studying flows at the IATP, National Academy of Sciences of Ukraine includes theoretical and experimental studies of the hydrodynamics and heat transfer of these flows and the development of new models and methods for their calculation. Particular consideration is given to the justification of the conditions for physical similarity, the investigation of the flow structures, the elucidation of the general laws of heat transfer in them, the investigation of the hydrodynamics of flows with different forms and laws of flow swirling, and the investigation of the influence of boundary conditions on the flow structure.

In the experimental study, axial-vane (AV) and screw (S) swirlers were used. To generalize the experimental data, we used the results of investigations conducted by other authors for twisted tape, tangential (T) and tangential-vane (TV) swirl, and snail conveyance (Sn). The vanes of the AV swirlers were contoured according to the exponential law ur^k = const, where u is the rotational velocity at the outlet from the swirler vanes. At a constant value of the axial velocity in the swirler cross-section the latter expression can be given in the following form $\tan\varphi = \tan\varphi_n (R/r)^k$, where R is the internal radius of the channel and φ_n is the angular twist of the blade on radius R. At $k = +1.0$ the law of constancy of circulation (of a "free" vortex) is realized, at $k = 0$ constancy of the angular twist φ along the radius is

Institute of Applied Thermal Physics, National Academy of Sciences of Ukraine, 2A Zhelyabov Str., Kiev, 03057, Ukraine; email: artem.khalatov@vortex.org.ua. Translated from Inzhenerno-Fizicheskii Zhurnal, Vol. 83, No. 4, pp. 743–756, July–August, 2010. Original article submitted January 20, 2010.

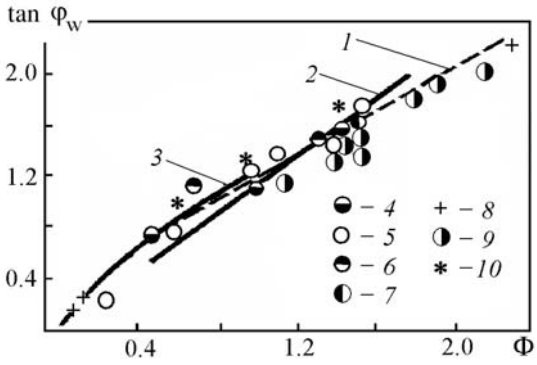

Fig. 1. Relation between the flow swirl parameters tan φ_w and Φ in the pipe [1, 2]: 1) generalizing equation (1); 2) inlet AV-swirler, at the inlet; l/d = 12, air (the author); 3) rotating propeller at the inlet, l/d = 10, water (the author); 4–7) experimental data of different authors [4] T-swirler, l/d = 18, air; 5) rotating section, l/d = 170, air; 6) T-swirler, l/d = 58, air; 7) T- and AV-swirlers, l/d = 58, air]; 8) T-swirler, l/d = 58; air; 9) AV-swirler, l/d = 12, air; 10) TV-swirler, l/d = 100, air.

provided, and at k = (–0.1) the law of rotation of a "solid" body (induced vortex) takes place. To justify the physical similarity of swirling flows, an additional series of studies with a rotating propeller with whirling water at the inlet to the tube was made.

Experimental measurements of the swirling flow structure made it possible to reveal that near the swirler ($x/d < 3$–4) the swirl of the flow "suppresses" turbulence and the flow becomes laminar with a system of Görtler vortices near the surface that are oriented along curved streamlines. Analysis of our own experimental data as well as of the results of other investigations made it possible to conclude that in the main portion of the channel ($x/d > 3$–4) the distributions of axial and rotational velocities are similar and depend on the local swirling intensity of the flow and the Reynolds number, and in the dimensionless form they depend only on the swirling intensity of the flow.

Analysis of our own experimental data as well as of the data obtained by other authors made it possible to establish that in the main portion of the channel in any of its cross-sections a universal relation between the integral parameter Φ and the local parameter tan φ_w of the swirl holds (Fig. 1). Here $\Phi = M/(K_x R)$ is the vorticity of the flow and tan φ_w is the angular swirl on the channel wall. Direct measurements have shown that both parameters characterize the similarity of the swirling flows and can be used to obtain universal dependences for the heat transfer and hydrodynamics of the swirling flow [1].

The general equation for different flow swirling techniques for liquid and gaseous media in a cylindrical channel has the form

$$\tan \varphi_w = 1.18\Phi^{0.76}. \qquad (1)$$

Exponential equations similar in structure that characterize the unique relation between the parameters Φ and tan φ_w were obtained for a tube with diaphragming of the outlet cross-section in convergent (confusers) and divergent (diffusers) axisymmetric channels.

The similarity of the swirling flows and the universal relation in form (1) are due to the universal relation between the axial and rotational velocity components in the main portion of the channel in the form $\bar{r}$ tan φ = const that holds in the region of $\bar{r} > 0.1$. Here tan $\varphi = u/w$ is the ratio between the rotational and axial velocities. The obtained results point to the fact that this law is universal and is formed in the main portion with different swirling techniques and mechanisms of liquids and gases.

The equations for calculating the angular swirl of the flow on the channel wall, the counterflow radius, and the radial and azimuthal nonuniformity of the flow in the region behind swirlers of various types are presented in [2]. The same paper considered also the generalization of the Rayleigh method to the case of translational-rotational motion of the flow. In general form, the condition for an active character of influence of the swirl on the flow structure is

defined by the inequality $[1 + 2k + (k + 1)\tan^2 \varphi][1 + 2k + \tan^2 \varphi]^{-1} > 0$. Choosing adequate values of k and φ, we can control the flow structure behind the swirler and, consequently, regulate the heat and mass transfer intensity. However, this control can only be realized at a distance from the swirler ($x/d < 3$–4) where the velocity distribution obeys the law of contouring the swirler vanes.

The structure of the boundary layer of the swirling flow for turbulent flow has been studied in detail in a cylindrical channel. The equations characterizing the axial and total velocity profiles in the region of the near-wall flow in universal coordinates of the boundary layer have the following form:

$$\varphi_x = 5.5 + 6.13\,(\Phi - 0.07)^{0.43} + [5.75 - 4.22\,(\Phi - 0.07)^{0.38}] \log \eta_x ,$$

$$\varphi_\Sigma = 5.5 + 4.65\,(\Phi - 0.07)^{0.26} + [5.75 - 3.36\,(\Phi - 0.07)^{0.30}] \log \eta_\Sigma .$$

Here $\varphi_x = w/w_*$, $\varphi_\Sigma = W/W_*$, $\eta_x = yw_*/\nu$, $\eta_\Sigma = yW_*/\nu$ denotes the universal coordinates of the boundary layer; $w_* = (\tau_{xw}/\rho)^{0.5}$, $W_* = (\tau_{\Sigma w}/\rho)^{0.5}$ are the axial and the total dynamic velocity; W is the total velocity of the swirling flow. The most appreciable deviation from the laws of the axial flow is observed in the range of $\Phi = 0.15$–0.50. On the basis of the generalization of experimental data equations characterizing the upper bound of validity of the "wall law" were obtained. In the boundary layer thickness, the ratio between the rotational and axial velocities of the flow tan φ is almost constant and equal to tan φ_w, and transition to the laws of the axial flow occurs at $\Phi \approx 0.07$ ($\varphi_w \approx 9^o$).

The investigations confirmed the theoretical conclusions about the mixed character of action of the flow swirl on its turbulence [1, 2]. In the main portion where the condition $\bar{r}$ tan φ = const is fulfilled, near the wall of the tube, a conservative action of the whirl on the flow and "suppression" of turbulent pulsations takes place, and in the central region the swirl has an active character with a high level of turbulent pulsations. As the swirl decays, the longitudinal and transverse pulsations of the flow near the wall increase, and in the central region they decrease; in so doing, the region of conservative action of the swirl expands.

As a result, the correlation coefficients have an alternating character in the cross-section of the channel, while being positive near the channel wall. The radial distribution of the correlation coefficient r_χ characterizing the relationship between the turbulent friction along the streamline and the kinetic energy of turbulence equals 0.25–0.30 near the surface of the channel and increases with decreasing vorticity of the flow. At a weak swirl ($\Phi < 0.10$) the correlation coefficient r_χ = 0.3–0.4, which is close to the laws of the axial flow.

The investigation of the conditions for physical similarity of swirling flows made it possible to obtain universal equations characterizing the local and integral parameters of swirling flows for arbitrary techniques and laws of initial swirling of the flow [1, 2]. In particular, for the differential static pressure and the total excess pressure averaged over the cross-section of the channel, the following equations were obtained:

$$\bar{P}/P_w = (1 + 1.77\Phi^{1.56}) , \quad \bar{P}^*/P_w = 1.08 - 0.1\Phi , \tag{2}$$

from which it follows that the differential static pressure on the channel wall is approximately equal to the cross-section-average total excess pressure.

To calculate the longitudinal change in the swirl parameter, the following equations were proposed:

$$\Phi/\Phi_{in} = \exp(-p_1 X) , \quad X < X_1 ; \tag{3}$$

$$\Phi/\Phi_{in} = \exp[(p_2 - p_1) X_1 - p_2 X] , \quad X > X_1 , \tag{4}$$

where $X_1 = 0.48 + 0.66\Phi_{in}$; $p_1 = 0.44 + 0.03\Phi_{in}$; $p_2 = 0.36 + 0.05\Phi_{in}$. These equations were obtained in the range of Φ_{in} = 0.4–2.5. Here $X = \bar{x}\mathrm{Re}_d^{-0.25}$ is a dimensionless coordinate, $\bar{x} = x/d$. On this basis the conditions and the coordinate of the transition of the swirling flow to an axial stabilized flow were determined [1].

A large series of studies was devoted to the influence of boundary conditions on the hydrodynamics of the swirling flow. Among them are investigations of the relative length of the channel, the partial swirl of the flow at the inlet to the channel (axial flow near the wall), the diaphragmed outlet cross-section of the tube, and flows in a conical

and a divergent channels in a Laval supersonic nozzle [1, 2]. A large base of new experimental data was obtained, equations characterizing the influence of boundary conditions on the heat transfer were presented, and local and integral parameters of the swirling flow were given. Diaphragming of the outlet cross-section leads to a decrease in the axial velocity near the wall and the formation of an intense vortex in the near-axis region of the channel due to the increase in the rotational velocity. In so doing, "suppression" of the longitudinal component of turbulence near the wall and in the near-axis vortex (laminarization of the flow due to the strong acceleration) takes place.

A large series of studies of the heat transfer in tubes of different lengths at various boundary conditions was made. For a tube of length 150 diameters with air swirled at the inlet by axial-vane swirlers in the range of variation of the angle φ_n from 15 to 60° and the exponent k from (−1) to (+3) for calculating the heat transfer the following equation was obtained:

$$\mathrm{Nu}_x = 0.0306\,\mathrm{Re}_{x\mathrm{m}}^{0.8}\,\mathrm{Pr}^{0.4}\varepsilon_\varphi\varepsilon_\mathrm{t}\,, \tag{5}$$

where $\varepsilon_\varphi = 1 + 0.49(\Phi - 0.19)^{0.61}$; $\varepsilon_\mathrm{t} = [2/(\sqrt{\psi + 1})]^{1.6}$; $\psi = T_\mathrm{w}/T_\mathrm{f}$ is the temperature factor.

In the given case, the Nusselt and Reynolds numbers in Eq. (5) are based on the axial distance x and the maximum axial velocity of the flow near the channel wall w_m [1], and the current value of the flow vorticity Φ is defined by Eqs. (3) and (4). From Eq. (5) it follows that at $\Phi < 0.19$ the heat transfer of the swirling flow practically corresponds to the heat transfer in the axial flow in the tube. For a tube of length 12 calibers, for the swirling factor (air) the equation $\varepsilon_\varphi = 1 + 0.44\Phi^{0.78}$ was obtained. This equation yields results close to the calculation by Eq. (5).

In [2], the equations for the factor of heat transfer with a flow swirled at the inlet by screw swirlers (air) and a rotating propeller (water) are given. For the flow strongly swirled by a screw swirler, the dependence $\mathrm{Nu} \sim \mathrm{Re}^{0.5}$ characteristic of a laminar flow was obtained, which points to the laminarization of the flow behind the screw (conservative action of the swirl).

In [1–3], on a single methodological basis, generalization of the published data for the main portion of the tube for the twisted tape, the tangential swirler, the tangential-slit swirler, and the axial-vane swirler with partial swirling at the inlet was carried out. Over 1000 experimental data were generalized by the single relation

$$\varepsilon_\varphi = 1 + 0.5\Phi^{0.75}\,,$$

which is a universal equation for various techniques and laws of initial swirling of the flow.

In a swirling flow in a tube, the energy losses consist of three components: friction loss in the channel, losses in the swirler, and outlet losses. The axial and tangential components of the surface friction are defined by the equations given in [1, 2]. Unlike the axial flow, hydraulic losses in a channel with a swirling flow are determined from the equation for calculating the energy loss characterized by the equation $E = E_\mathrm{in} \exp(-c\bar{x})$. Here E_in is the energy of the swirling flow behind the swirler; c is an exponent depending on Φ_in and l/d [1].

In [2], it was shown for the first time that in using the average value of the flow swirl at length l, the ratio f/f_a depends only on the average vorticity $\bar{\Phi}$ and does not depend on the Reynolds number and the relative length of the tube. On this basis, in air swirling by a screw at the inlet to a tube of length $l/d = 20$, we obtained the following generalized equation: $f/f_\mathrm{a} = 1 + 18.5(\bar{\Phi} - 0.19)^{1.43}$, where f_a is the hydrodynamical drag coefficient for a fully developed axial flow in the tube.

The energy loss of the swirling flow at the channel length l is determined from the equation $E_\mathrm{out} = E_\mathrm{in} \exp(-cl/d)$, and the outlet loss is determined by the coefficient $\xi_1 = 2E_\mathrm{out}/G\overline{w}^2$ [1]. The experimental dependences for calculating the pressure loss in swirlers of various types and at the outlet from tubes of various lengths are given in [1, 2].

For the case of local and extended swirls of the flow generated by different swirlers, their thermohydraulic characteristics were considered in [1–4]. Further investigations led to the idea of a modified Reynolds analogy [9]. The results of the analysis made it possible to draw the fundamental conclusion that the data for the Reynolds analogy factor for all known methods of heat transfer intensification lie between the data for a surface with specific recesses at small Reynolds numbers (upper limit) and the data for a ribbed surface at large Reynolds numbers (lower limit). It

was shown that the Reynolds analogy factor for swirling flows varies from 0.4 to 0.65 depending on the flow swirling technique.

In [1], we developed an approach to the relative friction and heat transfer laws in a swirling flow that takes into account the effects of increase in the flow velocity and curvature of the streamlines near the surface. The general equation for the heat transfer intensification factor ε_φ under conditions close to quasi-thermal ones has the following form: $\varepsilon_\varphi = \gamma_*^{1.6}\left(1 - \dfrac{b}{2\gamma_*}\right)^{-1.6}$, where $\gamma_* = (1 + \tan^2 \varphi_w)^{0.5}$; $b = 0.24 \tan \varphi_w^{0.46}$. The expression for the velocity profile in the boundary layer confirms the conclusion that in a swirling flow it is more "filled" than in the axial flow ($b/\gamma_* > 0$). For approximate calculations, in [2], an approach to the calculation of the heat transfer in a swirling flow on the basis of the "helical line of flow" theory was developed.

On the basis of experimental and theoretical investigations, as well as of the generalization of the majority of published data, we developed methods for calculating the heat transfer and the hydrodynamics of a swirling flow in impenetrable and porous tubes, circular channels, convergent and divergent channels, and Laval nozzles.

2. Convex and Concave Surfaces [5, 6]. At the IATP, NASU, the heat transfer and hydrodynamics near convex and concave surfaces have been investigated at various boundary conditions since 1987. Primary consideration is given to the justification of the condition for physical similarity, the investigation of the turbulent structure, the local and integral parameters of the boundary layer, and the influence of the longitudinal curvature, external turbulence, longitudinal pressure gradient, ingestion and exhaustion through the porous wall on the friction and heat transfer laws. The influence of the longitudinal curvature on the heat transfer and surface friction in a semirestricted stream and in film cooling of the surface has been investigated.

Curvature of the streamlines in flowing past a convex and a concave surfaces leads to the appearance of a transverse pressure gradient, i.e., the static pressure across the boundary layer becomes variable. The transverse pressure gradient transforms the velocity and temperature profiles in the boundary layer: near a convex surface they become less "filled," and near a concave surface — more "filled." One important property of a curved boundary layer is the active and conservative actions of mass forces on the flow structure. In the first case, in the flow Görtler vortices arise and turbulence develops, and in the second case, the field of mass forces prevents the development of turbulence and secondary flows. Convex curvature favors "later" laminar-turbulent transition compared to the flow on a flat surface, and concave curvature favors "earlier" transition.

The physical similarity of flows near a curved surface is characterized by the ratio δ^{**}/R_w = const. In specific cases, the ratio δ/R_w is used. For a semirestricted stream near a curved surface, the condition for physical similarity has the form δ_m/R_w = const.

For flows near curved surfaces in the absence of external actions (pressure gradient, turbulence, etc.), the similarity equations are as follows:

$$\mathrm{Nu}/\mathrm{Nu}_a = f_1(\delta^{**}/R_w), \quad C_f/C_{fa} = f_2(\delta^{**}/R_w), \tag{6}$$

where Nu_a, C_{fa} are the Nusselt number and the surface friction coefficient for the axial flow. For a semirestricted stream, in the brackets of Eq. (6) the simplex δ_m/R_w should be used.

The dimensionless velocity and temperature profiles in a curved boundary layer are described by the laws $w/w_f = \xi^{1/n}$, $\theta/\theta_f = \xi_t^{1/n_t}$, where $\xi = y/\delta$; $\xi_t = y/\delta_t$ and exponents n and n_t are functions of the similarity numbers δ^{**}/R_w or δ/R_w. The values of exponents n and n_t for the boundary layer near a convex surface are smaller than near a flat plate, and near a concave surface they are larger. In the range of variation of the curvature parameter δ^{**}/R_w from 0 to 0.0015, for the exponent n on a convex surface the following equation was obtained: $\dfrac{n}{n_a} = 1 - 0.191\left(\dfrac{\delta^{**}}{R_w} \cdot 10^3\right)^{0.452}$,

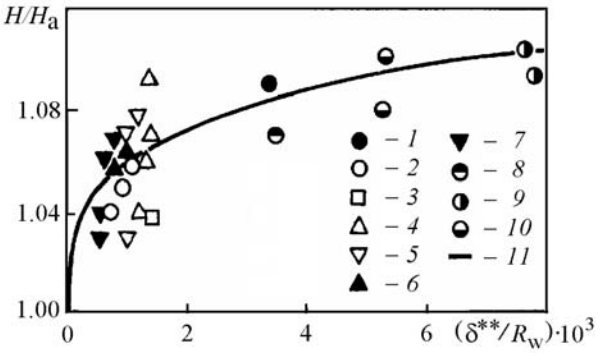

Fig. 2. Influence of the convex curvature of the surface on the value of the formparameter H [5, 6]: 1–10) experimental data of different authors; 11) equation for H_R.

where $n_a = 7$ corresponds to the axial flow. For the boundary layer near a concave surface, the exponent n has the following form ($n_a = 7$): $\frac{1}{n} = \frac{1}{n_a} + 1107.5\frac{\delta^{**}}{R_w} - 53{,}740\left(\frac{\delta^{**}}{R_w}\right)^2$.

The universal logarithmic laws characterizing the velocity and temperature profiles in a "curved" boundary layer, the equations for calculating the boundary of the viscous sublayer, and the laws of velocity and temperature defect in a curved boundary layer were considered in [5, 6].

Of great importance for practical calculations are the integral parameters of the boundary layer. In [5], it was shown that for the form factor H on a curved surface the superposition principle $H = H_a H_R$, where H_a is the form factor of the boundary layer near a flat wall, holds. The equation for the curvature factor H_R on a convex surface is of the form (Fig. 2)

$$H_R = 1 + 0.0593\left(\frac{\delta^{**}}{R_w}\cdot 10^3\right)^{0.28}.$$

As follows from the data presented in Fig. 2, in the region of $\frac{\delta^{**}}{R_w} \le 0.002$, the most appreciable change in the H_R value is observed.

On a concave wall, because of the increase in the filling of the velocity and temperature profiles in the boundary layer, the values of integral parameters decrease. For the concave curvature factor H_R, in the region of $\left|\frac{\delta}{R_w}\right| = 0 - 0.06$, the following equation was obtained: $H_R = 1 - 1.8\left|\frac{\delta}{R_w}\right|$. The influence of external turbulence on the local and integral parameters of a turbulent boundary layer was considered in [5].

As a consequence of the conservative action of the mass forces, the convex curvature decreases the normal quadratic pulsations in the boundary layer thicknesses. In the flow past a concave surface, the normal turbulent shear stresses increase, but this increase is especially noticeable in the case of a strong curvature ($\delta/R_w \approx 0.1$), where the normal stress exceeds the analogous data for a flat surface by a factor of two and more.

The turbulent shear stress on a convex wall is smaller and on a concave one greater than on a flat surface. At a large relative curvature of the boundary layer ($\delta/R_w \approx 0.1$) on the convex surface in the external part of the boundary layer the shear stress takes on a negative value, which points to the pulsation-to-average transition of the flow energy.

The influence of the boundary layer curvature on the surface friction and heat transfer is satisfactorily described by the equations following from the method of superpositions [5, 6]:

$$C_f/2 = (C_{fa}/2)\,\Psi_R, \tag{7}$$

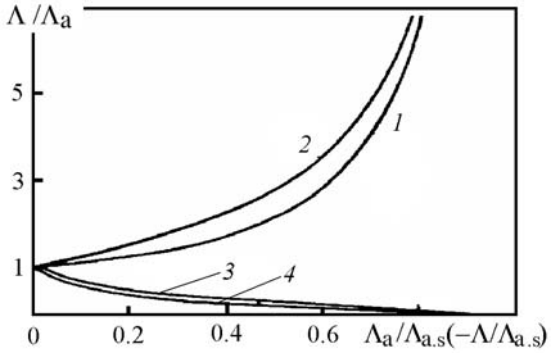

Fig. 3. Reynolds analogy coefficient on a flat and a convex surfaces: 1, 3) data of the author; 2, 4) flat plate [1, 2) $dP/dx > 0$; 3, 4) $dP/dx < 0$].

$$\mathrm{St} = \mathrm{St_a}\Psi_R^T . \tag{8}$$

The equations for calculating the relative friction and heat transfer functions in a zero-gradient flow have the following form:

on the convex wall

$$\Psi_R = [1 + 1000\ (\delta^{**}/R_\mathrm{w})]^{-0.12}, \quad \Psi_R^T = [1 + 1000\ (\delta^{**}/R_\mathrm{w})]^{-0.13}, \tag{9}$$

on the concave wall

$$\Psi_R = [1 + 756\ |\delta^{**}/R_\mathrm{w}|]^{0.15}, \quad \Psi_R^T = [1 + 756\ |\delta^{**}/R_\mathrm{w}|]^{0.14}. \tag{10}$$

Equations (10) reflect the surface-averaged values of Ψ_R and Ψ_R^T. The presence of Görtler vortices leads to a sinusoidal change in the friction and heat transfer coefficients in the transverse direction with an amplitude of ±20% as compared to the averaged value.

The external turbulence strongly influences the local and integral characteristics of the boundary layer. In [5], the representation of the form factor H in the form $H = H_\mathrm{a} H_R H_\mathrm{Tu}$, where the functions H_R and H_Tu reflect the influence of the curvature and external turbulence, was justified. The equations for determining the relative function H_Tu on the convex and concave surfaces are given in [5].

In the presence of additional factors, the friction and heat transfer coefficients can T calculated in accordance with the principle of superpositions. For example, at a simultaneous influence of the curvature and the external turbulence the computing equations have the following form: $C_\mathrm{f} = C_\mathrm{fa}\Psi_R\Psi_\mathrm{Tu}$, $\mathrm{St} = \mathrm{St_a}\Psi_R^T\Psi_\mathrm{Tu}^T$, where the functions Ψ_R and Ψ_R^T are defined by the equations characterizing the influence of curvature on the friction and heat transfer. The expressions for the relative functions Ψ_Tu and Ψ_Tu^T are given in [5, 6].

At a simultaneous influence of the curvature and the velocity gradient of the external flow, the principle of superposition of the curvature and the pressure gradient has the following form: $C_\mathrm{f} = C_\mathrm{fa}\Psi_R\Psi_\Lambda$, $\mathrm{St} = \mathrm{St_a}\Psi_R^T\Psi_\Lambda^T$. The expressions for the relative friction and heat transfer functions under acceleration and deceleration of the external flow are given in [5, 6].

An important feature of the flow at a positive pressure gradient is the separation of the boundary layer. On a curved surface, under the action of centrifugal forces the "filling" of the velocity profile changes, which affects the values of the separation parameters [5]. In particular, the separation value of the pressure gradient parameter $\Lambda_\mathrm{a.s}^R$ on a convex wall is determined by the formula $\dfrac{\Lambda_\mathrm{a.s}^R}{\Lambda_\mathrm{a.s}} = \left(1 + 1930\dfrac{\delta^{**}}{R_\mathrm{w}}\right)^{-0.13}$.

The closeness of the relative values of the friction Ψ_R and heat transfer Ψ_R^T factors (Eqs. (9) and (10)) points to the fulfillment of the Reynolds analogy on convex and concave walls in a zero-gradient flow past them. The lon-

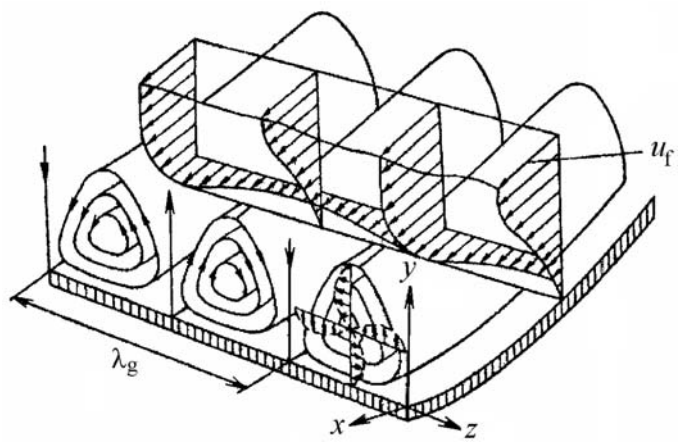

Fig. 4. Görtler vortices in the boundary layer.

gitudinal pressure gradient disturbs the analogy between the heat transfer and the friction in the boundary layer. The data for the Reynolds analogy coefficient in accelerated and slowed-down flows on the convex surface are presented in Fig. 3. As follows from the analysis of these data, they correspond, to an accuracy of ±5%, to the results obtained for the flat surface under the conditions of the longitudinal pressure gradient.

As mentioned above, on the concave surface, as a result of the centrifugal instability, in the boundary layer, Görtler vortex structures (Fig. 4) leading to a nonuniform distribution of the surface friction and heat transfer in the transverse direction arise. To calculate the critical Görtler value and the transition to a flow with Görtler vortices, we recommend the following equations in a laminar flow:

$$\delta/R_w = 0 - 0.02: \quad \ddot{G}o_{cr} = 22.97; \quad \delta/R_w > 0.02: \quad \ddot{G}o_{cr} = 22.76\,(\delta/R_w)^{0.05},$$

in a turbulent flow:

$$\ddot{G}o_{cr} = 2.21\cdot 10^3 - 6.68\cdot 10^4\,(\delta/R_w) + 7.73\cdot 10^5\,(\delta/R_w)^2 - 3.07\cdot 10^6\,(\delta/R_w)^3.$$

The equations for calculating the friction and heat transfer coefficients across the concave surface obtained in linear and nonlinear analyses have the following form:

$$C_f = C_{fR}\,[1 + g_1 \cos(\sigma z) + g_a], \quad \mathrm{St} = \mathrm{St}_R\,[1 + g_1^T \cos(\sigma z) + g_a^T].$$

Here C_{fR}, St_R are the surface friction coefficient and the Stanton number on the concave surface in the absence of Görtler vortices (Eqs. (7), (8), (10)); g_1, g_1^T, g_a, g_a^T are functions describing the linear and nonlinear influences of Görtler vortices on the surface friction and heat transfer [5, 6]. In the case of a laminar flow, these functions have an order of 70–100%, and for a turbulent flow — 10–20%. The data of the analysis of the influence of external turbulence and the longitudinal pressure gradient on the centrifugal instability, the critical Görtler number, and the wave number are given in [5, 6].

The velocity profile in the near-wall region of a semirestricted stream ($y < \delta_m$) is described by the power law $w/w_m = (y < \delta_m)^{1/n}$, where the exponent n for the convex and concave surfaces is defined, respectively, by the equations $n/n_a = 1 - 1.7(\delta_m/R_w)^{0.31}$ and $n/n_a = 1 + 2.69(\delta_m/R_w)^{0.65}$. In the jet part of the profile ($y > \delta_m$), whatever the sign of the surface curvature, the velocity profile is satisfactorily described by the hyperbolic dependence [5]. The dimensionless temperature profile in the jet region is described by the power law $\theta/\theta_f = (\delta/\delta_T)^{1/m}$, where the exponent n on the concave surface has the following form: $m/m_a = 1 + 4.4(\delta_m/R_w)^{0.56}$, where $m_a = 12.0$.

The longitudinal curvature has a weak effect on the friction coefficient near convex and concave surfaces. It has a stronger influence on the heat transfer. We obtained the following equations for the heat transfer coefficient on convex and concave surfaces:

$$\mathrm{Nu}_x/\mathrm{Nu}_{xa} = 1 - 0.088\,[(\delta_m/R_w)\cdot 10^3 - 0.5]^{0.81}, \quad \mathrm{Nu}_x/\mathrm{Nu}_{xa} = 1 + 4.15\,[(\delta_m/R_w) - 0.002]^{0.65},$$

where Nu_{xa} is the equation for the heat transfer in the axial flow of the semirestricted stream near a flat surface.

The specific features of the influence of the velocity and temperature profiles curvature lead to a change in the efficiency of film cooling on convex and concave surfaces. The current value of the efficiency of film cooling on the convex surface is higher and on the concave one lower than on the flat surface. To calculate the film cooling efficiency, we recommend the equation $\eta = \eta_a \varepsilon_R$, where η_a is the efficiency of film cooling on the flat surface; $\varepsilon_R = \left(1 + 0.24\mathrm{Re}_s^{-0.25}\frac{x}{m_b s}\right)^{0.8}\left(1 + 0.24\mathrm{Re}_s^{-0.25}\Psi_R\frac{x}{m_b s}\right)^{-0.8}$ is the correction for the surface curvature; Re_s is the Reynolds number for the cooling stream. The curvature factor Ψ_R in this equation is defined by Eqs. (9) and (10). The relation between the film cooling efficiency for discrete η_d (for which the above relation was obtained) and the efficiency of slit η_{sl} supply of the coolant is defined by the equation $\eta_d = 0.714\eta_{sl}$.

To determine the film cooling efficiency on a convex surface under flow acceleration, we recommend the following equation: $\eta_{R,\Lambda} = \eta_a \varepsilon_R \varepsilon_\Lambda$, where η_a is the film cooling efficiency on the flat surface; ε_R is the surface curvature factor; $\varepsilon_\Lambda = (w_f/w_{in})^{-0.19}$ is the flow acceleration factor.

The results of the investigations made promoted the development of models and methods for calculating curved flows that take a more accurate account of the influence of the surface curvature on the laws of heat and momentum transfer in the boundary layer. We developed a theory of the boundary layer for the flow and heat transfer near a convex and a concave walls, justified the mathematical models for calculating the flow and heat transfer in a zero-gradient and a gradient flow, developed linear and nonlinear approaches to the analysis of the centrifugal instability, and justified the principle of superposition of individual actions for calculating complex curved flows.

The criteria for flow separation were justified, and methods for calculating the flow and heat transfer for a semirestricted stream and the efficiency of film cooling near a convex and a concave surfaces under the conditions of external flow acceleration and external turbulence were elaborated.

3. Surface-Vortex Systems [3]. The research program of the IATP, NASU in the field of surface-vortex systems was set up in 2001 with a focus on the investigation of the heat transfer and hydrodynamics at low Reynolds numbers when the effects of surface-vortex structures are the most significant. In the program, the following configurations were investigated: a single recess, single, double, and triple rows of recesses of various forms, circular pipes with external transverse flow past them, and channels with surface recesses and projections blocking up the cross-section. On the basis of the investigations made, a diagram of flow conditions was constructed, justification of the Reynolds analogy was carried out, and new vortex technologies were developed. Below, the principal results of the investigations made are considered.

As early as the 1950–1960s, it had been revealed in experiments that surface recesses are not normal asperities but represent an independent class of vortex flows with unique thermohydraulic characteristics. It had been revealed that at sufficiently large Reynolds numbers in a deep spherical recess ($h/D > 0.26$) a nonstationary vortex oscillating in the angular direction was formed and was periodically ejected into the external flow. Observations had shown that the physical structure of this phenomenon was close to the "constricted" natural tornado; therefore, vortex structures generated by spherical recesses were named "tornado" vortices. Subsequently, it was revealed that the vortex form was largely determined by the external flow conditions.

Primary consideration in the research program of the IATP, NASU was given to the investigation of the physical structure in systems with "shallow" (h/D = 0.05–0.10) spherical and cylindrical recesses on a flat surface. The main experiments were performed at the Air Force Academy of the USA (in a water pipe) in the range of variation of the average velocity in the working portion 0.05–0.5 m/s. The recess diameter D was 50.8 mm, the depth h was 2.54 and 5.08 mm, and the Reynolds number Re_D constructed along the recess diameter was varied over the range 3200–24,500. The flow before the recess remained laminar. In experiments, the flow was visualized with the help of colored water, and the field velocities were measured by means of a two-component laser anemometer.

Measurements of the velocity profile before the recess showed that on the symmetry axis, as well as at a distance $z = \pm D/2$ from the axis in the transverse direction, the velocity profile corresponds to the shear flow, whereas

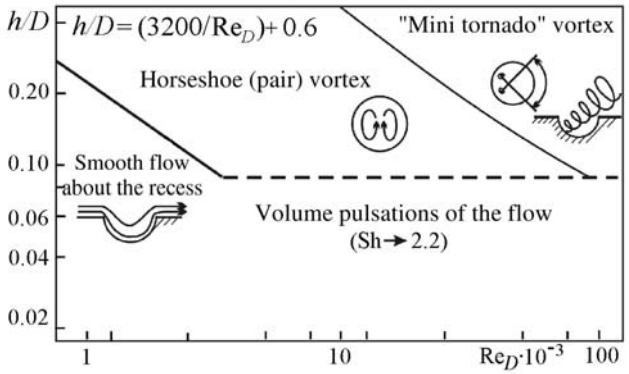

Fig. 5. Diagram of vortex structures in a single spherical recess.

in the interval between them ($z = \pm D/4$) it is essentially nonuniform with height and time. This is due to the upstream influence of the nonstationary oscillations formed inside the recess.

Among the previously unknown features of the vortex structure of the flow, the change of the sense of rotation of the twin vortex inside the cylindrical recess at $\mathrm{Re}_D > 15{,}000$, as well as the formation of an asymmetric fluctuating "vortex wake" behind the spherical recess at small Reynolds numbers, are noteworthy. Another specific feature is a considerable "delay" in the onset of twin vortex shedding with increasing thickness of the boundary layer before the recess. In general, the boundary layer thickness plays an important part in the formation of the flow structure inside recesses.

The depth of the separation zone in the cylindrical recess is larger than in the spherical one and increases with increasing initial thickness of the boundary layer. A particularly rapid increase in the separation zone in the cylindrical recess is observed in the range of variation of the Reynolds number Re_D from 5000 to 10,000, both at small and large initial thickness of the boundary layer. An increase in the latter "shifts" the incipience of the flow separation in the recess towards higher Reynolds numbers, and, noteworthily, this "shift" is the most significant for the spherical recess.

Generalization of the experimental data on the flow structure in a single spherical recess was carried out on the basis of a large body of published experimental data and is given in Fig. 5. As is evident from the experimental data [4], in a "shallow" recess ($h/D < 0.10$), in a wide range of Reynolds numbers the flow fluctuations have a volume-vortex character, and the boundary of transition to the structure of the flow with a twin and a pulsating vortex ("mini tornado" vortex) has a curvilinear form.

At a small thickness of the boundary layer the transition to turbulence behind the cylindrical recess is observed somewhat earlier ($\mathrm{Re}_D > 6600$) than behind the spherical one ($\mathrm{Re}_D > 8000$). As the boundary layer thickness increases, the laminar-turbulent transition behind the spherical and cylindrical recesses occurs at $\mathrm{Re}_D > 12{,}250$ and $\mathrm{Re}_D > 8000$, respectively. Thus, for the "smoother" spherical form the boundary layer thickness weakly influences the conditions for the transition to turbulence behind the recess.

It was revealed that unlike "deep" recesses, fluctuations of the flow behind "shallow" recesses ($h/D \le 0.10$) are volume-vortex in nature and lead to periodic ejections into the main stream of large volumes of the liquid from the flow separation region. For the investigated range of Reynolds numbers, the change in the Strouhal number Sh is described by a curve with a maximum (Fig. 6). As is evident from the data obtained [4], there is no considerable difference between cylindrical recesses of depth $h/D = 0.05$ and $h/D = 0.10$. The maximum value of the Strouhal number for the spherical recess is somewhat lower than for the cylindrical one and is shifted towards higher Reynolds numbers. An increase in the boundary layer thickness before the recess decreases the frequency of fluctuations behind the recess. For the cylindrical recess, this influence disappears at $\mathrm{Re}_D > 16{,}000$–$17{,}000$, and for the spherical one it disappears at $\mathrm{Re}_D > 24{,}000$. In general, the absolute values of the Strouhal number in the investigated range of Reynolds numbers are fairly high and exceed considerably its values in the separation region of the cross-streamlined cylinder.

The investigation of the heat transfer behind a single spherical and a single cylindrical recesses ($h/D = 0.10$) by the liquid-crystal method has shown that the thermal "wake" behind the recess reaches 5–6 diameters of the recess,

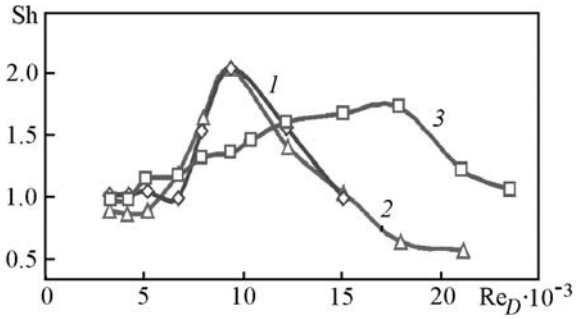

Fig. 6. Volume pulsations of the flow of water behind the recess (x/D = 1.23): 1, 2) cylindrical recess (h/D = 0.10 and 0.05); 3) spherical recess (h/D = 0.10).

while the technically important intensification of the heat transfer is observed at a distance of 2–3 diameters from the rear edge of the recess. Convex and concave surfaces are characterized by an active and a conservative influence of centrifugal forces on the flow structure and the heat transfer. The average heat transfer in a recess on the concave wall is higher and in a recess on the convex wall lower than on the flat surface. However, experiments revealed no influence of the surface curvature on the pulsation frequency of the vortex in a single recess.

The main feature of the single row of recesses is the nonuniformity of the flow field in the transverse direction because of the free space between recesses. The specific features of the flow structure in the single-row system of "shallow" recesses (h/D = 0.10) are described in detail in [3]. Here we note that at small Reynolds numbers the frequency of volume fluctuations of the flow behind the cylindrical recess in the single row is close to the values for a single cylindrical recess, and in the range of Re_D from 8000 to 12,000 the Strouhal number behind the recess in the single row is lower than behind the single cylindrical recess.

At $Re_D > 10{,}200$ the frequency of pulsations behind a recess in the row is already higher by 30–40% than that of pulsations generated by a single cylindrical recess, and adjacent recesses begin to produce a marked influence on the fluctuations frequency of the flow only at $Re_D > 8000$. In general, the Strouhal number behind the spherical recess in the single row is higher by about 10% than for the single spherical recess. Thus, unlike the cylindrical form of the recess, the presence of recesses adjacent to spherical recesses produces a stronger effect on the intensity of flow fluctuations.

Visualization of the flow showed that adjacent recesses have no appreciable influence on the depth (in the longitudinal direction) of the separation zone on the symmetry line; however, these recesses influence the behavior of peripheral streamlines, changing the form of the separation zone and making it narrower compared to the separation zone for a single recess. At $Re_D > 10{,}500$ all configurations, except for the "shallowest" single cylindrical recess (h/D = 0.05), have an approximately equal depth of the separation zone, with the depth of the separation zone in a recess with h/D = 0.05 at Re_D = 20,000 constituting 80%.

The presence of adjacent recesses in the row strongly influences the form of the separation zone: at high Reynolds numbers ($Re_D > 10{,}000$) the separation zone has the form of a sector for both cylindrical and spherical recesses and is approximately equal in both cases. At low Reynolds numbers the separation zone of the flow also has the form of a sector, with the spherical recess in the row having a narrower zone.

For the investigated conditions (S_x/D = 1.50), the transition to turbulence behind a recess in the single row occurs at approximately the same values of the Reynolds number as for a single recess ($Re_D > 6600$ for the cylindrical form and $Re_D > 8000$ for the spherical form).

The periodically repeated double row of recesses on a flat surface can be considered as an alternative to multirow systems of recesses. The flow structure and the volume fluctuations behind the two-row system of recesses of spherical and cylindrical forms were investigated with the example of "shallow" recesses (h/D = 0.10). Recesses were staggered so that their centers formed an isosceles triangle with the side and base equal to the transverse step S_z = 76.2 mm. The longitudinal step of recesses S_x was equal to 88 mm.

The flow structure in a second-row recess is influenced by adjacent recesses, as well as by above recesses between which there is a space for free motion of the flow. Thus, the vortex structure of the second row interacts with

vortices generated by the first row of recesses. The presence of adjacent recesses produces a marked effect on the transition to turbulence in the two-row system. Behind a recess of the second row for the cylindrical form the transition to turbulence is observed somewhat earlier ($Re_D > 6000$) than for a single recess, and for the spherical form, somewhat later ($Re_D > 9500$). Investigations carried out for the cylindrical form showed that the presence of recesses of the second row leads also to an increase in the critical Reynolds number of the laminar-turbulent transition behind a recess of the first row ($Re_D > 8100$).

The heat transfer and the surface friction behind the double row of recesses of spherical, cylindrical, rhombic, or quadratic forms (h/D = 0.20 and 0.30) were investigated for the air flow in a rectangular channel. The recesses were arranged in staggered order so that their centers formed an isosceles triangle with the base equal to the transverse step S_z. The relative step in the longitudinal direction S_x/D = 0.44 and the transverse direction S_z/D = 2.0. The boundary layer thickness before the system of recesses was no more than 1.0 mm.

The results of the investigations showed that for the investigated configurations turbulent conditions arise practically immediately behind the two-row system ($Re_* > 3000$). For all configurations, the obtained data are in good agreement with the equation for turbulent flow on a plate approximated into the region of low Reynolds numbers. This point to a weak influence of the form of the recess on the heat transfer at a group arrangement of recesses. The highest intensification of the heat transfer (Nu_x/Nu_{xa} at Re_x = const) equals 3.55 and is observed for cylindrical recesses with h/D = 0.20.

The measurement data for the surface friction behind the double row of recesses show that the data obtained immediately behind a recess (x_*/D = 1.2–1.8) lie between the data for laminar and turbulent flows. This is due to the partial "deformation" of the near-wall velocity profile behind the rear edge of the recess. At a distance x_*/D = 4.16–4.56 the experimental data for the surface friction are in good agreement with the line for the turbulent flow on the plate. The obtained results point to a stronger influence of the surface recesses on the velocity profile than on the temperature profile near the system of recesses.

The results of the investigation of the triple row of "shallow" recesses (h/D = 0.10) show that the transition to turbulence behind the cylindrical and spherical recesses of the third row occurs at $Re_D > 9400$. Thus, after the third row the form of the recess practically does not influence the value of the critical Reynolds number. In the three-row system, behind the cylindrical recess of the second row the transition to turbulence occurs at $Re_D > 5250$–6800. This agrees approximately with the data obtained for the cylindrical recess in the second row in the two-row system of recesses ($Re_D > 6000$).

The previous experiments with multiple recesses on a flat surface made it possible to draw an important conclusion about the "self-organization" of nonstationary vortices coordinating their space-time behavior in accordance with the conditions for the flow past the surface. Such a structure at a high density of recesses provides a fairly high intensification factor of heat transfer (Nu/Nu_a = 2.7–2.9) accompanied by about the same increase in the pressure loss.

The experimental program was carried out in the region of small Reynolds numbers when the external flow contains no vorticity "suppressing" recess-generated volume fluctuations. In the investigations, spherical recesses on both surfaces of the channel were used. The ratio of the channel height to the recess diameter H/D was 0.175 ("narrow" channel), at which vortices emerging from the recesses do not get into the flow core but join the channel wall.

The experiments were performed in an open wind tunnel of the IATP, NASU. The "narrow" rectangular channel was of height B = 2.1 mm, width A = 56 mm, and length L = 156 mm. In experiments, the Reynolds number Re_{eq} was varied in equivalent size of the channel from 770 to 26,500. The spherical recesses with a sharp edge (13–17 rows depending on the density of recesses γ) were arranged in staggered order on either surface of the rectangular channel. Their diameter and depth were 12.0 and 2.4 mm (h/D = 0.20), respectively, and the density γ was 67, 55, and 40%.

According to the obtained data, the Nusselt number in the channel with surface recesses exceeds the data for the smooth channel. In the range of variation of the number Re_{eq} from 900 to 10,000, it is proportional to the Reynolds number to power 0.74 ($Nu_{eq} \sim Re_{eq}^{0.74}$), and at $Re_{eq} > 10{,}000$, to power 0.8 ($Nu_{eq} \sim Re_{eq}^{0.8}$). A change in the density of recesses γ from 40 to 55% practically does not influence the heat transfer intensity. However, a further increase in the density (to 67%) leads to a marked intensification of the heat transfer throughout the range of variation of the Reynolds number. At γ = 67% the ratio Nu_{eq}/Nu_a reached its maximum value of 3.7 at $Re_{eq} \approx 2400$, whereas the ratio f/f_a was only 2.25 (Fig. 7a). Such intensification is much higher that at high Reynolds numbers [4], where

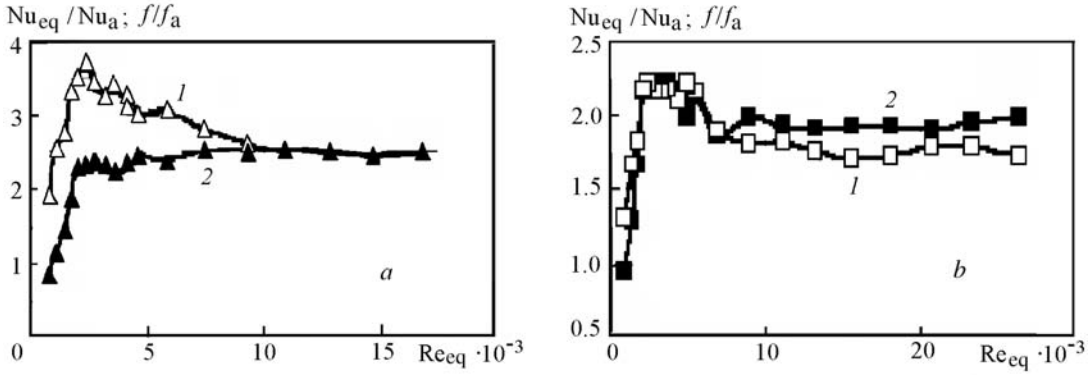

Fig. 7. Average heat transfer and pressure loss in a channel with spherical recesses on both surfaces (h/D = 0.20): a) γ = 67%; b) 55%; 1) Nu/Nu_a; 2) f/f_a.

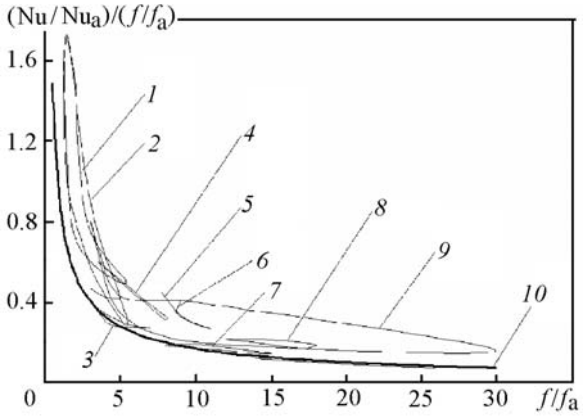

Fig. 8. Reynolds analogy: 1) spherical recesses on two sides of the channel; 2) spherical recesses on one side of the channel; 3) internal grooves; 4) spherical projections on a flat surface; 5) 60-degree continuous and split ribs; 6) 90-degree split ribs; 7) alternating spherical projections and recesses; 8) internal spiral groves; 9) spherical recesses and projections on the sides of a plane channel (close contact); 10) limiting curve of the surface ribbing at large Reynolds numbers.

the maximum heat transfer intensification is 2.5–2.8. In the region of $Re_{eq} < 10{,}000$, the heat transfer intensification exceeds the increase in the drag, i.e., here the Reynolds analogy factor exceeds 1. At $Re_{eq} > 10{,}000$ the ratios Nu_{eq}/Nu_a and f/f_a become approximately equal. At γ = 55% the heat transfer intensification corresponds approximately to the increase in the drag up to Re_{eq} = 6000–7000 (Fig. 7b). The maximum value of Nu_{eq}/Nu_a = 2.3 is also attained at $Re_{eq} \approx 2400$.

The generalization of the published base of experimental data for channels with spherical recesses on one or two sides of a rectangular channel showed that for various geometric and regime parameters of the channel its thermohydraulic efficiency $(Nu/Nu_a)/(f/f_a)^{0.33}$ is always higher than 1 and varies from 1.0 to 2.4, i.e., such systems are energetically advantageous under all conditions. The ratio $(Nu/Nu_a)/(f/f_a)$ in the form of the Reynolds analogy factor is also used for estimating the thermohydraulic efficiency of the system. However, a more graphical analysis is attained by using the Reynolds analogy factor when for the coordinate axis the ratio $(Nu/Nu_a)/(f/f_a)$ and for the abscissa axis the ratio f/f_a are used [3].

Figure 8 presents in $(Nu/Nu_a)/(f/f_a)$ vs. f/f_a coordinates the experimental data for various methods of heat transfer intensification. Analysis of these results leads to the fundamental conclusion that the experimental data for all known methods of heat transfer intensification lie in the region between the results for surface ribbing at large Reynolds numbers (curve 10) and the data for spherical recesses at small Reynolds numbers (curve 2). Consequently,

the condition for faster intensification of the heat transfer $\mathrm{Nu}/\mathrm{Nu}_a > f/f_a$ is attained only in the region of small values of the ratio f/f_a = 1.25–2.5.

Since the flow hydrodynamics in surface-vortex systems is nonstationary, the main method for obtaining equations for its calculation is the physical experiment. In [3], the empirical equations for calculating the surface friction, the hydrodynamical drag, the heat transfer, and the thermohydraulic efficiency for various configurations of surface-vortex systems are given.

Conclusions. The investigations conducted have made it possible to develop significantly the concepts in the area of heat transfer and hydrodynamics in the fields of mass forces of various nature, as well as develop new mathematical models, methods, and computer programs for calculating swirling flows, vortex, and curved flows widely used in the design organizations in Ukraine and Russia. They were also adopted at the University of Cardiff (Great Britain), the Air Force Academy of the USA, and in the companies Rolls-Royce (Great Britain) and Solar Turbines (USA).

The data obtained promoted the creation of new vortex technologies of aerothermodynamics protected by the author's certificates and patents of Ukraine and Russia. Among them are cyclone cooling of gas turbine blades, passive control of the flow separation near airfoils under conditions other than the calculated ones, oscillating film cooling of gas turbine blades, heat transfer surfaces with high thermohydraulic characteristics, heat exchangers and recuperators for microturbines and metallurgy, low-toxicity combustion chambers, etc. A detailed description of the new vortex technologies is given in [7].

NOTATION

A, width of the channel, m; B, height of the channel, m; $C_f/2 = \tau_w/(\rho w_f^2/2)$, surface friction coefficient; $C_{fR}/2$, surface friction coefficient on a concave surface in the absence of Görtler vortices; c, exponent in the equation for the swirling flow energy; C_p, isobaric heat capacity, J/(kg·K); d, diameter of the channel, m; D, surface recess diameter, m; $E = 2\pi \int_0^R P^* w r dr$, swirling flow energy, N·m/s; E_{in}, swirling flow energy at the outlet from the swirler, N·m/s; E_{out}, swirling flow energy at the outlet from the channel, N·m/s; $f = 2\Delta P_w/(\rho \overline{w}^2)(l/d)$, hydrodynamical drag coefficient of the swirling flow; G, mass flow, kg/s; $\mathrm{G\ddot{o}} = \mathrm{Re}_x\sqrt{\delta/R_w}$, Görtler similarity number; g_1, g_a, functions describing the linear and nonlinear influence of Görtler vortices on the surface friction coefficient; g_1^T, g_a^T, functions describing the linear and nonlinear influence of Görtler vortices on the heat transfer; $H = \delta^*/\delta^{**}$, form factor of the boundary layer; h = recess depth, m; $K_x = 2\pi \int_0^R \rho w^2 r dr$, momentum flux, N; k, exponent in the law of twist of swirler vanes; l, cylindrical channel length, m; L, plane channel length, m; $M = 2\pi \int_0^R \rho u w r^2 dr$, flux of angular momentum, N·m; $m_b = (\rho w)_s/(\rho w)_f$, coolant blow parameter; m, exponent for the temperature profile in the boundary layer; $\mathrm{Nu}_x = \alpha x/\lambda$, Nusselt number along the channel length x; $\mathrm{Nu}_{eq} = \alpha(2B)/\lambda$, Nusselt number along the equivalent diameter of the channel; n, exponent for the flow velocity profile in the boundary layer; Pr, Prandtl number; P, differential static pressure, Pa; P^*, differential total pressure, Pa; P_w, differential statis pressure on the channel wall, Pa; $\overline{P}$, differential static pressure averaged over the cross-section of the channel, Pa; $\overline{P}^*$, differential total pressure averaged over the cross-section of the channel, Pa; ΔP, pressure loss on length l, N/m^2; r, current radius, m; p_1, p_2, exponents in Eqs. (3) and (4); $\overline{r} = r/R$, dimensionless radius; R_w, radius of curvature of a convex or concave surface, m; $\mathrm{Re}_x = w_f x/\nu$, Reynolds number on the longitudinal coordinate; $\mathrm{Re}_{xm} = w_m x/\nu$, Reynolds number for the maximum velocity; $\mathrm{Re}_D = w_f D/\nu$, Reynolds number on the recess diameter; $\mathrm{Re}_d = w_f d/\nu$, Reynolds number on the channel diameter; Re^{**} =

$w_f\delta^{**}/\nu$, Reynolds number in the momentum thickness; $Re_{eq} = \overline{w}2B/\nu$, Reynolds number on the equivalent diameter; $Re_s = w_s s/\nu$, Reynolds number on the height of the slit s; $Re_* = w_f x_*/\nu$, Reynolds number at the x_* coordinate; r_χ, correlation coefficient; $Sh = fD/\overline{w}$, Strouhal number; S_x, S_z, longitudinal and transverse step of recesses, m; $St = \alpha/C_p w_f \rho$, Stanton number; St_R, Stanton number on a concave surface in the absence of Görtler vortices; s, height of the film cooling slit, m; T, temperature, K; T_w^*, adiabatic wall temperature, K; T_s, coolant temperature, K; u, w, v, rotational, axial, and radial velocity components, m/s; $\overline{w}$, axial velocity averaged over the cross-section of the channel, m/s; w_f, longitudinal velocity component in the flow core, m/s; w_s, coolant velocity at the outlet from the slit, m/s; w_{in}, flow velocity at the inlet to the channel, m/s; w_m, maximum flow velocity, m/s; x, z, longitudinal and transverse coordinates, m; x_*, downstream distance from the rear edge of the recess, m; y, normal distance from the wall, m; α, heat transfer coefficient, W/(m^2·K); γ, density of recesses, %; δ^{**}, momentum thickness, m; δ^*, displacement thickness, m; δ, boundary layer thickness, m; δ_T, thermal boundary layer thickness, m; $\eta = (T_f - T_w^*)/(T_f - T_s)$, film cooling efficiency; η_d, film cooling efficiency (discrete supply); η_{sl}, film cooling efficiency (slit supply); $\theta = T - T_w$, current temperature difference, deg; $\theta_f = T_f - T_w$, temperature pressure, deg; $\Lambda_{a.s}^R$, parameter of the pressure gradient on a convex wall; $\Lambda_{a.s}$, parameter of the pressure gradient on a flat wall; λ, heat conductivity coefficient, W/(m·K); λ_g, wavelength of Görtler vortices. m (Fig. 4); ν, kinematic viscosity, m^2/s; ξ, dimensionless distance (dynamic boundary layer); ξ_t, dimensionless distance (thermal boundary layer); ξ_1, relative energy losses of the swirling flow in the channel; ρ, density, kg/m^3; σ, wave number, 1/m; τ_{xw}, surface friction in the longitudinal direction, N/m^2; $\tau_{\Sigma w}$, total surface friction, N/m^2; Φ, integral parameter of the flow swirl; $\overline{\Phi}$, length-l-average parameter of the flow swirl; $\varphi = \arctan(u/w)$, angular twist of the flow, deg; φ_n, angular twist of the swirler vanes at $r = R$, deg; φ_w, angular twist of the flow on the channel wall, deg; Ψ_R, relative friction function (curvature) at $Re^{**} = const$; Ψ_R^T, relative heat transfer function (curvature) at $Re^{**} = const$; Ψ_{Tu}, relative friction function (turbulence) at $Re^{**} = const$; Ψ_{Tu}^T relative heat transfer function (turbulence) at $Re^{**} = const$; Ψ_Λ, relative friction function (pressure gradient) at $Re^{**} = const$; Ψ_Λ^T, relative heat transfer function (pressure gradient) at $Re^{**} = const$. Subscripts: a, axial flow parameters; in, parameters at the channel inlet (swirler outlet); out, parameters at the channel outlet; d, discrete blow; cr, critical parameter; t, thermal; eq, equivalent; sl, slit; f, parameters in the flow; s, parameters at the slit outlet; Tu, turbulence; w, parameters on the channel wall; φ, swirl.

REFERENCES

1. V. K. Shchukin and A. A. Khalatov, *Heat Transfer, Mass Transfer, and Hydrodynamics of Swirling Flows in Axisymmetric Channels* [in Russian], Mashinostroenie, Moscow (1982).
2. A. A. Khalatov, *Theory and Practice of Swirling Flows* [in Russian], Naukova Dumka, Kiev (1989).
3. A. A. Khalatov, I. V. Shevchuk, and A. A. Avramenko, *Heat Transfer and Hydrodynamics in the Fields of Centrifugal Mass Forces*, Vol. 3, *Swirling Flows* [in Russian], IATP, NAS of Ukraine, Kiev (2000).
4. A. A. Khalatov, I. I. Borisov, and S. V. Shevtsov, *Heat Transfer and Hydrodynamics in the Fields of Centrifugal Mass Forces*, Vol. 5, *Heat Transfer and Thermohydraulic Efficiency of Vortex and Swirling Flows* [in Russian], IATP NAS of Ukraine, Kiev (2005).
5. A. A. Khalatov, I. V. Shevchuk, and A. A. Avramenko, *Heat Transfer and Hydrodynamics in the Fields of Centrifugal Mass Forces*, Vol. 1, *Curved Flows* [in Russian], IATP, NAS of Ukraine, Kiev (1996).
6. A. A. Khalatov, I. V. Shevchuk, A. A. Avramenko, S. G. Kobzar', and T. A. Zheleznaya, *Thermal Gas Dynamics of Complex Flows Near Curved Surfaces* [in Russian], IATP, NAS of Ukraine, Kiev (1999).
7. A. A. Khalatov, *Heat Transfer and Hydrodynamics in the Fields of Centrifugal Mass Forces*, Vol. 7, *Vortex Technologies of Aerothermodynamics in Power Gas Turbine Manufacture* [in Russian], ITTF, NAS of Ukraine, Kiev (2008).
8. A. A. Khalatov and A. S. Kovalenko, *Heat Transfer and Hydrodynamics in the Fields of Centrifugal Mass Forces*, Vol. 6, *Heat Transfer and Hydrodynamics of Accelerated Flow in Plane Curvilinear Channels* [in Russian], Naukova Dumka, Kiev (2006).
9. A. A. Khalatov, I. V. Shevchuk, and A. A. Avramenko, *Heat Transfer and Hydrodynamics in the Fields of Centrifugal Mass Forces*, Vol. 2, *Rotating Systems* [in Russian], IATP, NAS of Ukraine, Kiev (1996).